UCRL-JC--105437

DE91 005070

Computational Model for Optimizing Longitudinal Fin Heat Transfer in Laminar Internal Flows*

C. S. Landram

Lawrence Livermore National Laboratory
Livermore, California 94550

* Work performed under the auspices of the U.S. Department of Energy by the Lawrence Livermore National Laboratory under Contract W-7405-Eng-48.

Nomenclature

b_1	channel half-width
b_2	fin half-width
D_h	channel hydraulic diameter
h	local heat transfer coefficient, $q_w/(T_w - T_b)$
H	channel height
k	thermal conductivity
q_w	base heat flux at lower surface
Q	total heat flow to each cell, below Eq. (1)
S	defined by Eq. (2)
T	temperature
y	dimensionless, y'/b
y'	lateral dimension
z	dimensionless, z'/H
z'	longitudinal dimension
θ	dimensionless temperature defined below Eq. (1)
λ	defined by Eq. (6b)
ε	defined by Eq. (11)
ϕ	dimensionless fin to coolant heat flux, Eq. (9)

Subscripts:

w	at coolant-fin or base interface
1	coolant
2	fin
B	base
b	bulk of coolant

Abstract

Optimal configurations are identified, based on a numerical model, for fully developed laminar internal flows whose base boundary walls have perpendicular fins extending longitudinally into the fluid. The optimum coolant flow channel, formed between each fin, has an aspect ratio dependent on the coolant to wall thermal conductivity ratio and on the fin to channel width ratio, which is optimally about unity. A base thickness exists which minimizes the base hot-spot temperature, and its value is dependent on the fin to channel width ratio.

Introduction

The multiple fin-channel-base configuration shown in Fig. 1a, used for heat exchanger and electronics cooling designs[1], has laminar channel coolant flow into the plane of the figure. The heat load enters uniformly along the bottom surface of the base and flows predominantly up the fins and convects to the coolant. Some heat is convected directly from the top of the base to the coolant. The tops of the coolant channels and fins are adiabatic.

Thermal analysis[2,3,4] of the problem is complicated by the thermal coupling (conjugation) between the fin and coolant and the base and coolant. These couplings render highly non-uniform interfacial heat transfer coefficients which are unknown a priori and which depend in a sensitive and complicated fashion on the problem geometry (e.g., on b_1/a and b_2/b_1 in Fig. 1a) and on the ratio of fluid to wall thermal conductivity k_1/k_2.

In absence of the base, a numerical study[2] was performed assuming an isothermal base-coolant interface with all heat entering the bottom of the fins, and an exact solution was obtained[3] for a similar situation except that the base-coolant interface was assumed adiabatic (instead of isothermal). Both calculations assumed hydrodynamically and thermally developed velocity and temperature profiles and uniform heat flux in the direction of fluid flow. Reference 3 revealed the existence of an optimum aspect ratio (channel width to height) minimizing fin root temperature.

One numerical study[4] considered a single base-fin-coolant configuration of Fig. 1a with fully developed flow and uniform heat flux at the wall. The parameters were not varied and the results were not of particular value for optimization. Base

thickness, a most important parameter in determining peak hot-spot temperature, was not considered.

In the present study a computational model is presented which allows parametric variations in channel, fin and base region sizes. A series of verification problems, including the case for which an exact solution[3] holds, is described and to which the numerical results are tested. Results are optimized with respect to aspect ratio, channel to fin width ratios, base thickness to channel half-width ratios and coolant to wall thermal conductivity ratios. Fully developed laminar flows with uniform heat flux at the wall and constant properties are considered.

Formulation

The fluid flow into the plane of the coolant passage of Fig. 1a is laminar and is hydrodynamically and thermally developed. All properties are taken constant, and the imposed heat flux q_w on the lower surface of the base is taken uniform in the (axial) direction of coolant flow. At any axial station, the local energy equation, in terms of the normalized coordinates y, z of Fig. 1b, is given by:

$$\frac{\partial^2\theta}{\partial y^2} + \left(\frac{b_1}{H}\right)^2 \frac{\partial^2\theta}{\partial z^2} = S(y,z) \qquad (1)$$

where the dimensionless temperature θ is related to its dimensional value T by

$$\theta = \frac{T - T_b}{\frac{Q}{2k_1}\frac{b_1}{H}}$$

$$Q = 2b_1 \int_{\frac{-b_2}{b_1}}^{1} q_w dy$$

and T_b is the fluid bulk temperature.

In Eq. (1), S is zero in the base and fin regions and in the coolant passage it is the ratio of the local fluid velocity to the mean velocity. Reference 3 demonstrated that accurate assessments of fin temperature and fin-fluid heat flux could be obtained using the approximate velocity ratio:

$$S(y,z) = g(y)\, f(z),\ 0 < y < 1,\ 0 < z < 1 \qquad (2)$$

where

$$g(y) = \frac{3}{2}[1 - (1 - y)^2]$$

$$f(z) = \left\{1 - \cosh\left[\frac{2}{\gamma}\left(z - \frac{1}{2}\right)\right] \Big/ \cosh\left(\frac{1}{\gamma}\right)\right\} \Big/ \delta$$

$$\gamma = 2\sqrt{\frac{2}{5}}\ \frac{b_1}{H}$$

$$\delta = 1 - \gamma \tanh\frac{1}{\gamma}$$

The fluid bulk temperature at any axial position is known from the overall increase in bulk enthapy between the inlet and the particular axial location. It follows that

$$\int_0^1 \int_0^1 S(y,z)\,\theta(y,z)\,dydz = 0 \tag{3}$$

The boundary conditions around the computational domain of Fig. 1b are all of the Neumann type — zero θ gradients normal to the fin and channel centerlines of symmetry and zero gradients normal to the top, adiabatic surface. On the lower surface of the base, the heat flux q_w is specified, and, in terms, of the dimensionless variables this requires

$$\frac{-\dfrac{\partial\theta_B}{\partial z}}{\dfrac{k_1/k_B}{(b_1/H)^2}} = \frac{q_w}{\displaystyle\int_{\frac{-b_2}{b_1}}^{1} q_w dy} = \frac{1}{1+\dfrac{b_2}{b_1}}, \qquad z = \frac{-\delta_B}{H}, \quad \frac{-b_2}{b_1} < y < 1, \tag{4}$$

the latter equality holding if q_w is also independent of lateral position y (as well as axial position). Subscripts 1, 2 and B on dimensionless temperature and properties respectively refer to the fluid, fin and base regions. Henceforth q_w will be assumed independent of lateral position y.

Defining a laterally averaged fin temperature as

$$\bar{\theta}_2(z) = \frac{1}{\frac{b_2}{b_1}} \int_{-\frac{b_2}{b_1}}^{0} \theta_2(y,z)\, dy, \tag{5}$$

where $\theta_2(y,z)$ is described by Eq. (1) with $S = 0$. The "fin equation" is obtained by lateral integration of Eq. (1) across the fin's half-thickness, yielding

$$\lambda\left(\frac{\partial \theta_1}{\partial y}\right)_{y=0} + \frac{d^2\bar{\theta}_2}{dx^2} = 0 \tag{6a}$$

where

$$\lambda = \frac{H^2}{b_1 b_2} \frac{k_1}{k_2} \tag{6b}$$

Expanding a Taylor's series about the fin's centerline $y = - b_2 / b_1$ at any longitudinal position gives

$$\theta_2(y,z) = \theta_2\left(\frac{-b_2}{b_1}, z\right) + \frac{1}{2} \frac{k_1}{k_2} \frac{1}{b_2 / b_1} \frac{\partial \theta_1}{\partial y}(0,z) \left(\frac{b_2}{b_1} + y\right)^2 + O\left(\frac{b_2}{b_1} + y\right)^3 \tag{7}$$

which satisfies the appropriate boundary conditions at $y = - \frac{b_2}{b_1}$ and $y = 0$. In Table 1, the centerline to surface temperature drop across the fin determined from Eq. (7), ignoring the terms of order higher than two, is shown to closely match the corresponding exact values for the particular case analyzed in Reference 1 (no direct base-fluid heat transfer). The comparison shows that Eq. (7) is within about 1% of the

exact solution for the parameter $\varepsilon = \frac{k_1 b_2}{k_2 b_1} < 0.1$ and is within less than 0.1% for $\varepsilon < 0.01$.

Performing the indicated integration of Eq. (5) using Eq. (7) permits Eq. (6a) to be written as

$$\frac{\varepsilon}{3}\frac{d^2\phi}{dz^2} - \lambda\phi + \frac{d^2\theta_w}{dz^2} = 0 \tag{8a}$$

where $\phi(z)$ is the dimensionless interfacial heat flux

$$\phi(z) = -\frac{\partial\theta_1}{\partial y}(o,z) \tag{9}$$

and $\theta_w(z)$ is the dimensionless interfacial temperature with

$$\theta_w(z) \equiv \theta_1(o,z) \tag{10}$$

with

$$\varepsilon = \frac{k_1}{k_2}\frac{b_2}{b_1} . \tag{11}$$

Equation (8a) is the conjugated boundary condition applied to the fluid on y = 0, 0 < z< 1. With exception of base to fin conduction, no other consideration need be given the fin since fin-coolant coupling is incorporated into (8a). Once Eqs. (1), (2) and (8a) are solved, the fin temperature distribution can be recovered from Eq. (7).

Computational Methods

In Fig. 1b the entire base, $- b_2 / b_1 < y < 1$, $- \delta_B / H < z < 0$, and the lower portion of the fin/coolant region in $0 < z < z^*$ were resolved using finite differences. The upper fin/coolant region in $z^* < z < 1$ was resolved using an integral method. The finite difference calculations were linked to those based on the integral method along a longitudinal line $z = z^*$. The value for z^* (of order 0.1) was chosen large enough to resolve base-coolant conjugate heat flow from the finite difference mesh used in the coolant, the criterion being solution convergence as z^* is parametrically increased. Further elaboration follows.

A. Finite Difference Calculations in $- \delta_B / H < z < z^*$

i Base

For the base of Fig. 1b, Eq. (1) with $S = 0$ was centrally differenced using a variably sized mesh. The Neumann-type boundary conditions encountered along the symmetry line $y = - b_2 / b_1$ and $y = 1$ in $- \delta_B / H < z < 0$ of the base and along the lower surface of the base (Eq. (4)) were treated with second-order accuracy using the fictitious nodal point (Shih[5]) or interior point (Roach[6]) method. At the base-coolant interface, $z = 0$, $0 < y < 1$ and at the base-fin interface $z = 0$, $- b_2 / b_1 < y < 0$, the conservative forms of Eq. (1) were used (with harmonic differencing) as described by Patankar[7].

ii Coolant and Coolant-Fin Interface

For the fin interface and the coolant in $0 < z < z^*$, where the finite different calculations were applied, it was only necessary to solve Eqs. (1) and (2) in the coolant region, not the fin since boundary conditions (8a) applied, as previously discussed in the formulation. Since the resulting calculations are obtained for fin or base thermal conductivities up to several orders of magnitude greater than that of the coolant, it was necessary to use a fine mesh for the coolant near the walls (to as small as Δz or $\Delta y = .005$) with coarser meshing elsewhere in the coolant. The applicable Neumann-type condition on $y = 1$, $0 < z < z^*$ for the fluid was treated similar to those on the base as previously discussed.

iii Coolant-fin Boundary Condition

The finite difference representation of the fin-coolant boundary condition (8a) along $0 < z < z^*$, at $y = 0$, is now considered. The subscript 1, denoting the fluid, will be omitted here and the subscript W for wall, W + 1 for the first node in the fluid adjacent to the wall will instead be used.

Expanding ϕ (Eq. (9)) in a power series of ε

$$\phi = A + \varepsilon B + \varepsilon^2 C + \cdots ,$$

and then substituting back into Eq. (8a), one obtains the coefficients A, B, C, ..., to write as an alternative to (8a)

$$\phi = \frac{1}{\lambda}\left[\frac{d^2\theta_w}{dz^2} + \frac{\varepsilon}{3\lambda}\frac{d^4\theta_w}{dz^4} + O\left(\frac{\varepsilon}{3\lambda}\right)^2\right] \tag{8b}$$

A fictitious fluid node inside the fin has the temperature

$$\theta_{w,-1} = \theta_{w,+1} + 2\,\Delta y\,\phi + O(\Delta y^3)$$

and, therefore, the second-order central difference

$$\frac{\partial^2\theta_w}{\partial z^2} = \frac{2}{\Delta y^2}\left[\theta_{w,+1} - \theta_w + \frac{\Delta y}{\lambda}\phi\right] + O(\Delta y^2)$$

can be combined with Eqs. (8b) and (1) to give, along $y = 0$:

$$\left[\left(\frac{b_1}{H}\right)^2 + \frac{2}{\lambda\Delta y}\right]\frac{d^2\theta_w}{dz^2} + \frac{2}{\Delta y^2}(\theta_{w+1} - \theta_w) + \frac{2}{\lambda\Delta y}\frac{\varepsilon}{3\lambda}\frac{d^4\theta_w}{dz^4} + O(\Delta y)^2 + O\left(\frac{\varepsilon}{3\lambda}\right)^2 = 0\ . \tag{12}$$

Equation (12) provides a second order-accurate boundary condition at the fin-fluid interface, and was proven extremely useful in the limit that the ratio of the fin thickness $2b_2$ to fin height H is small:

$$\frac{\varepsilon}{3\lambda} = \frac{1}{12}\left(\frac{2b_2}{H}\right)^2 << 1\ .$$

B. <u>Application of the Integral Method in $z^* < z < 1$</u>

The fluid in $0 < y < 1$ is assumed to have the temperature distribution

$$\theta_1(y,z) = \theta_w(z) - \phi(z)\,G(y) \tag{13}$$

where ϕ and θ_w are defined by Eqs. (9) and (10) and apply here to $z^* < z < 1$. The function G(y) has the properties

$$G(o) = \frac{dG}{dy}(1) = 0$$

$$\frac{dG}{dy}(0) = 1$$

An appropriate choice for G is one which at least would satisfy the special problem for which θ_w and ϕ are independent of z:

$$G(y) = y - \frac{1}{2}\left(1 - \frac{y}{4}\right) y^3 \tag{14}$$

As in all applications of the integral method, the profile chosen (Eqs. (13) and (14)) is not required to satisfy the local fluid energy Eqs. (1) and (2) but rather is only required to satisfy the energy equation in the integral sense.

Integrating Eq. (1) with respect to y from the interface y = 0 to channel centerline y = 1 gives

$$\phi + \left(\frac{b_1}{H}\right)^2 \left[\frac{d^2\theta_w}{dz^2} - \frac{2}{5}\frac{d^2\phi}{dz^2}\right] = f(z) \tag{15}$$

where f(z) is given in Eq. (2). Combining Eq. (8a) and (15) by eliminating θ_w gives a single, linear second order ordinary differential equation describing ϕ:

$$\frac{\partial^2 \phi_w}{\partial z^2} - m^2\phi + Ko\,\phi(z) = 0 \qquad (16)$$

Once ϕ is known, θ_w is obtained from (8a):

$$\frac{d^2\theta_w}{dz^2} = (\lambda - m^2\frac{\varepsilon}{3})\,\phi + \frac{\varepsilon}{3} Ko\, f(z) \qquad (17)$$

where

$$m^2 = [1 + \lambda (\frac{b_1}{H})^2]\, Ko$$

$$Ko = [(\frac{b_1}{H})^2\ (\frac{\varepsilon}{3} + \frac{2}{5})]^{-1}$$

In considering the boundary conditions for Eqs. (16) and (17), Eq. (13) is differentiated to give

$$\frac{\partial\theta_1}{\partial z} = \frac{d\theta_w}{dz} - G(y)\frac{d\phi}{dz} \ .$$

Since $\frac{\partial\theta_1}{\partial z} = 0$ for all y at z = 1, the requirements that

$$\frac{d\theta_w}{dz} = \frac{d\phi}{dz} = 0 \quad \text{at } z = 1 \qquad (18)$$

must hold. The boundary conditions at $z = z^*$ are implied by the solution to the finite difference equations in $z < z^*$ and the coupling between the solutions to (16) and (17) for ϕ and θ_w in $z > z^*$.

The solutions to Eqs. (16) and (17) using (18) are given by

$$\phi = A\phi_a + \phi_b + \phi_c \tag{19}$$

and

$$\theta_w = (\lambda - m^2 \frac{\varepsilon}{3}) \left[\frac{(A\phi_a + \phi_b)}{m^2} + \theta_{w_a} + c_1 z\right] + c_2 \tag{20}$$

where A is an integration constant found by linkage at $z = z^*$ and c_1 is obtained from (18). The functions ϕ_a, ϕ_b, ϕ_c and θ_{w_a} are given in the appendix along with c_1.

The constant c_2 in Eq. (20) is obtain from Eq. (3). Using Eqs. (13) and (14) one obtains

$$\int_0^{z^*} \int_0^1 S\theta_1 dy dz + \int_{z^*}^{z} f(z) \left(\theta_w(z) - \frac{17}{35}\phi(z)\right) dz = 0 \tag{21}$$

where the first term is obtained by numerically integrating the finite difference output θ_1, and the second term is evaluated using integration by parts. The value for c_2 then becomes an element of the solution matrix from which θ_1 in $0 < z < z^*$ is determined.

C. Linkage of Computational Schemes at $z = z^*$

Nodal points along the longitudinal line $z = z^*$ joining the finite difference and integral method procedures were placed in the fluid and on the wall. Nodal fluid

temperatures along $z = z^*$, based upon the differenced expression for Eq. (1), depended on the values above z^*, say at $z^* + \Delta z$. Fluid temperatures above z^* were evaluated from Eqs. (13), (19) and (20), once the integration constant A appearing in the later two are known.

The interfacial fin/fluid temperature $\theta_w(z^*)$ at the joining longitudinal position was differenced according to Eq. (12), which introduces values of $\theta_w(z^* + \Delta z)$, $\theta_w(z^* + 2\Delta z)$, etc. The values of θ_w for $z > z^*$ were evaluated using Eq. (20). The single integration constant A was obtained by equating $\theta_w(z^*)$ found by Eq. (12) to that given by Eq. (20). Thus, the constant A, similar to c_2 discussed previously, was allowed to participate as a member of the solution matrix of unknowns.

Verification of Computational Model

Three separate verifications were made in which simpler cases of Fig. 1 were compared to known, corresponding solutions. First, the fin-coolant coupling (Eq. (12)) was tested by omitting the presence of the base, applying the heat flux $q_w (b_1 + b_2)/b_2$ at $z = 0$ uniformly to the root of the fin in $- b_2/b_1 < y < 0$ and imposing an adiabatic base-coolant interface at $z = 0$ in $0 < y < 1$. In Fig. 2, the exact solution[3] for the centerline fin temperature and fin-coolant interfacial heat flux are shown to compare closely to the numerical results for the case illustrated. The close agreement is also demonstrated in fin center root temperature as a function of aspect ratio as shown by the curves of Fig. 3 at each particular thermal conductivity ratio.

The second test was for base to coolant thermal coupling. Here Eq. (1) applied to the base and to the fluid was solved exactly when all lateral dependencies in y were ignored (fin absent). The function S in Eq. (1) was evaluated at $y = 1$. The maximum

error between the numerical solution, which is based on interfacial thermal conductivity harmonic averaging[7], and the exact solution was found to be less than 0.35%.

The final verification test problem was that for the two dimensional heat flow in the base region for various base thicknesses. An exact, two-dimensional solution to Eq. (1) applied to the base region was derived (see appendix) for the case of an adiabatic coolant-base interface at $z = 0$, $0 < y < 1$, with a uniform flux $q_w (b_1 + b_2)/b_2$ at the fin-base interface at $z = 0$, $- b_2/b_1 < y < 0$. The two upper curves of Fig. 4 compare exact and numerical solutions. The maximum difference between the two is less than .8% and is attributed primarily to slight non-uniformities in longitudinal heat flux at the fin-base interface calculated by the numerical model, but ignored (as a boundary condition) for the exact solution.

Results

All results are presented for the base and fin having the same thermal conductivity. The dependence of fin and base temperatures and Nusselt numbers on base boundary conditions is illustrated in Figs. 5 and 6. Case I[3] ignores the presence of the base and prescribes the heat flux q_w (1 + b1/b2) directly to the bottom of the fin. Cases II and III include two-dimensional heat flow in the base. Case II ignores interfacial base to coolant heat transfer, and Case III treats the actual conjugate base-fluid heat transfer as herein formulated. In all cases fin-coolant heat transfer is conjugated.

The fin-temperature near $z = 0$ for Cases II and III decreases from that determined from Case I (Fig. 5) as a result of the lateral temperature gradient in the

base (Fig. 6), which is negative for Cases II and III, positive for Case I. The fin temperature (Fig. 5) for the conjugate base-coolant interface (Case III) decreases from that for the adiabatic base-coolant interface (Case II) owing base-coolant heat leakage since less heat is transferred to the bottom of the fin.

The direct base-coolant heat leakage increases with increasing thermal conductivity ratio (Fig. 7) and explains the increasing difference between conjugated fin root temperature and fin root temperature for an adiabatic base-coolant interface (Fig. 3).

The longitudinal temperature distribution in the base, shown in Fig. 7, has the hot-spot (maximum) value at the bottom of the base, $z' = -\delta_B$, at the channel centerline, $y' = b_1$. The hot-spot base temperature and the fin root temperature are plotted as a function of the ratio of base thickness to fin spacing in Fig. 4. Their conjugated values (Case III) are lower than those determined from the adiabatic base-coolant case (Case II). The minimum in hot-spot base temperature with the base thickness shown in Fig. 4 is a consequence of lateral thermal resistance vs longitudinal thermal resistance in the base as its thickness increases.

The base hot-spot temperature normalized by $q_w b_1/k_1$ is plotted in Fig. 9 as a function of the fin to channel half-width ratio b_2/b_1 for the respective aspect ratio minimizing the root temperature (see Table 1, Fig. 3).
The ordinates of Fig. 9, based on a conductivity ratio of $k_1/k_2 = 0.005$, are minimized at $b_2/b_1 = 1$ for all base thicknesses. The minimum in hot-spot temperature also occurs at $b_2/b_1 = 1$ for other thermal conductivity ratios.

TABLE 1.

Dimensionless lateral fin temperature drop between the centerline and fluid interface at longitudinal midheights z = 1/2. Aspect ratio b_1/a chosen to maximize channel heating, and direct base to fluid heat transfer suppressed as in Ref. 1.

$$\theta_2\left(\frac{-b_2}{b_1}, \frac{1}{2}\right) - \theta_w\left(\frac{1}{2}\right)$$

$\frac{k_1}{k_2}$	$\frac{b_2}{b_1}$	ε	$\left(\frac{b_1}{a}\right)_{opt}$	$-\frac{\partial\theta_1}{\partial y}\left(0,\frac{1}{2}\right)$ (Exact)	Ref. 3 (Exact)	Eq. (7) (Approx.)	Error, $\left(\frac{\text{Exact - Eq. (7)}}{\text{Exact}}\right) \times 100$ (%)
.005	0.50	.0025	.16	1.102	.0013765	.0013772	- .05
	1.00	.005	.115	1.074	.0026830	.0026834	- .035
	2.00	.010	.081	1.051	.005257	.0052578	- .015
.05	0.50	.025	.50	1.110	.013899	.013994	- .68
	1.00	.050	.35	1.155	.028597	.028875	- .97
	2.00	.100	.24	1.139	.056338	.056943	- 1.07
.50	0.50	.250	1.24	0.826	.105035	.103296	+ 1.66
	1.00	.500	0.85	0.923	.232814	.23065	+ 0.93
	2.00	1.00	0.55	1.011	.49780	.505387	+ 1.52

TABLE 2.

Fin temperature insentivity to linkage line. The case shown is for $b_2/b_1 = 0.25$, $2\,b_1/H = .23$ and $k_1/k_2 = .005$. Base to fluid heat transfer suppressed[3].

		Error, Numerical - Exact Linkage Point in z		
z	$\frac{2b_1}{H}\theta_w$[3] (Exact)	0.125	.150	.20
0	.2360	0	.0002	.0009
.03	.2250	0	.0002	.0009
.10	.2026	- .0001	.0001	.0009
.30	.1454	- .00004	.0001	.0007
.50	.1034	- .00003	.0001	.0007
.70	.0772	- .00005	.0001	.0007
1.0	.06491	- .00004	.0001	.0007

References

1. F. Incropera, "Convection Heat Transfer in Electronic Equipment Cooling," ASME J. Heat Transfer 110, pp. 1097 -1111 (1988).

2. E. Sparrow, B. Baliga and S. Patankar, "Forced Convection Heat Transfer from a Shrouded Fin Array with and Without Tip Clearance," ASME J. Heat Transfer 100, pp. 572 - 579 (1978).

3. C. Landram, "An Exact Solution for Conjugate Longitudinal Fin-Fluid Heat Transfer in Internal Flow Including Optimization," UCRL-JC-103249, March 1990.

4. S. Lau, L. Ong, J. Han, "Conjugate Heat Transfer in Channels with Internal Longitudinal Fins," J. Thermophysics 3, pp. 303 - 308 (1989).

5. T. Shih, Numerical Heat Transfer, Hemisphere Publ. Corp., Washington, p. 149 (1984).

6. P. Roach, Computational Fluid Dynamics, Hermosa Publishers, Albuquerque, p. 147 (1972).

7. S. Patankar, "A Numerical Method for Conduction in Composite Materials, Flow in Irregular Geometries and Conjugate Heat Transfer," Proceedings International Heat Transfer Conference 3, pp. 297 - 302 (1978).

8. H. Carslaw and J. Jaeger, Conduction of Heat in Solids, 2nd Edition, Oxford Univ. Press., p. 463 (1959).

APPENDIX 1

Solutions to Equations (16) and (17)

The solutions to Eqs. (16) and (17) are given by Eqs. (19) and (20), respectively, where

$$\phi_a = \cosh mz - (\tanh m) \sinh mz$$

$$\phi_b = -\frac{2Y \sinh (\frac{1}{\gamma})}{\gamma m \cosh m} \sinh mz$$

$$\phi_c = X + Y \cosh [\frac{2}{\gamma}(z - \frac{1}{2})]$$

$$\theta_{wa} = \frac{X}{2} z^2 + \frac{Y}{(\frac{2}{\gamma})^2} \cosh [\frac{2}{\gamma}(z - \frac{1}{2})]$$

$$c_1 = (\gamma - m^2 \frac{\varepsilon}{3}) \{\frac{\gamma}{2} [(\frac{2}{\gamma m})^2 - 1] Y \sinh (\frac{1}{\gamma}) - X\}$$

$$X = \frac{Ko}{\gamma m^2}$$

$$Y = \frac{Ko}{\delta[(\frac{2}{\gamma})^2 - m^2] \cosh \frac{1}{\gamma}}$$

Symbols not identified here are given in the text.

APPENDIX 2

Base Temperature Distribution with Adiabatic Base-Coolant Interface, Uniform Flux at Base-Fin Interface

Equation (1) applied to the base region $-\frac{\delta_B}{H} < z < 0, -\frac{b2}{b1} < y < 1$ has $S = 0$ with boundary condition (4) at $z = -\frac{\delta_B}{H}$ and at $z = 0$, the flux $q_w\,(1 + \frac{b_1}{b_2})$ is assumed uniform in $-\ b_2/b_1 < y < 0$ and zero in $0 < y < 1$. The symmetry conditions at $y = -\frac{b_2}{b_1}$ and $y = 1$ permit a finite fourier cosine transform[8] with respect to the variable y. The result is given by

$$\theta - \theta_{Root} = \frac{4\,\frac{k_1}{k_2}}{\frac{b_1}{a}} \left\{ \frac{-z}{\frac{2(b_1 + b_2)}{H}} + \left(\frac{b_2}{b_1 + b_2}\right) \sum_{n=1}^{\infty} \Gamma_n \left[\cosh\left(\frac{n\pi\delta_B}{b_1 + b_2}\right) \right.\right.$$

$$\left.\left. - \cosh\left(\frac{n\pi H\,(z + \frac{\delta_B}{H})}{b_1 + b_2}\right) \cos\left(\frac{n\pi b_1\,(y + \frac{b_2}{b_1})}{b_1 + b_2}\right) \right] \right\}$$

where

$$\Gamma_n = \frac{1}{(n\pi)^2} \frac{\sin\left(\frac{n\pi b_2}{b_1 + b_2}\right)}{\sinh\left(\frac{n\pi\delta_B}{b_1 + b_2}\right)}$$

$$\theta_{Root} = \theta\left(-\frac{b_2}{b_1}, 0\right)$$

$$\theta_{Hot\text{-}spot} = \theta\left(1, \frac{-\delta B}{H}\right)$$

Figure 1a. Physical domain in plane of coolant flow showing actual coordinates y', z'.

Figure 1b. Hybrid computational domain. Finite difference computations in $-\delta_B/H < z < z^*$ are linked to integral method representations in $z^* < z < 1$. Dimensionless coordinates are $y = y'/b_1$ and $z = z'/H$.

Figure 2. Fin temperature and heat flux distributions for heat supplied to bottom of fin. Base coolant interface is adiabatic.

Figure 3. Fin root temperature. Adiabatic vs conjugated base-coolant interface.

Figure 4. Base hot-spot and fin root temperature dependencies on base thickness. Adiabatic vs conjugated base-coolant interface. Same parameters as on Fig. 2.

Figure 5. Fin temperature and Nusselt number. ADI is adiabatic base-coolant interface. Same parameters as on Fig. 2.

Figure 6. Base temperature and Nusselt number lateral distributions. Case nomenclature and parameters same as on Figs. 2 and 5.

Figure 7. Fraction of total power $q_w\,(b_1 + b_2)$ convected directly from the base to the coolant (by-passing fin). Aspect ratio $\frac{b_1}{a}$ evaluated at minimum fin root temperature.

Figure 8. Longitudinal temperature distribution in the base-fin region. Same parameters as in Fig. 2.

Figure 9. Base hot-spot temperature vs fin to channel half width ratio. The channel aspect ratio used is that minimizing fin root temperature. Thermal conductivity ratio = 0.005.

Fig 1
c

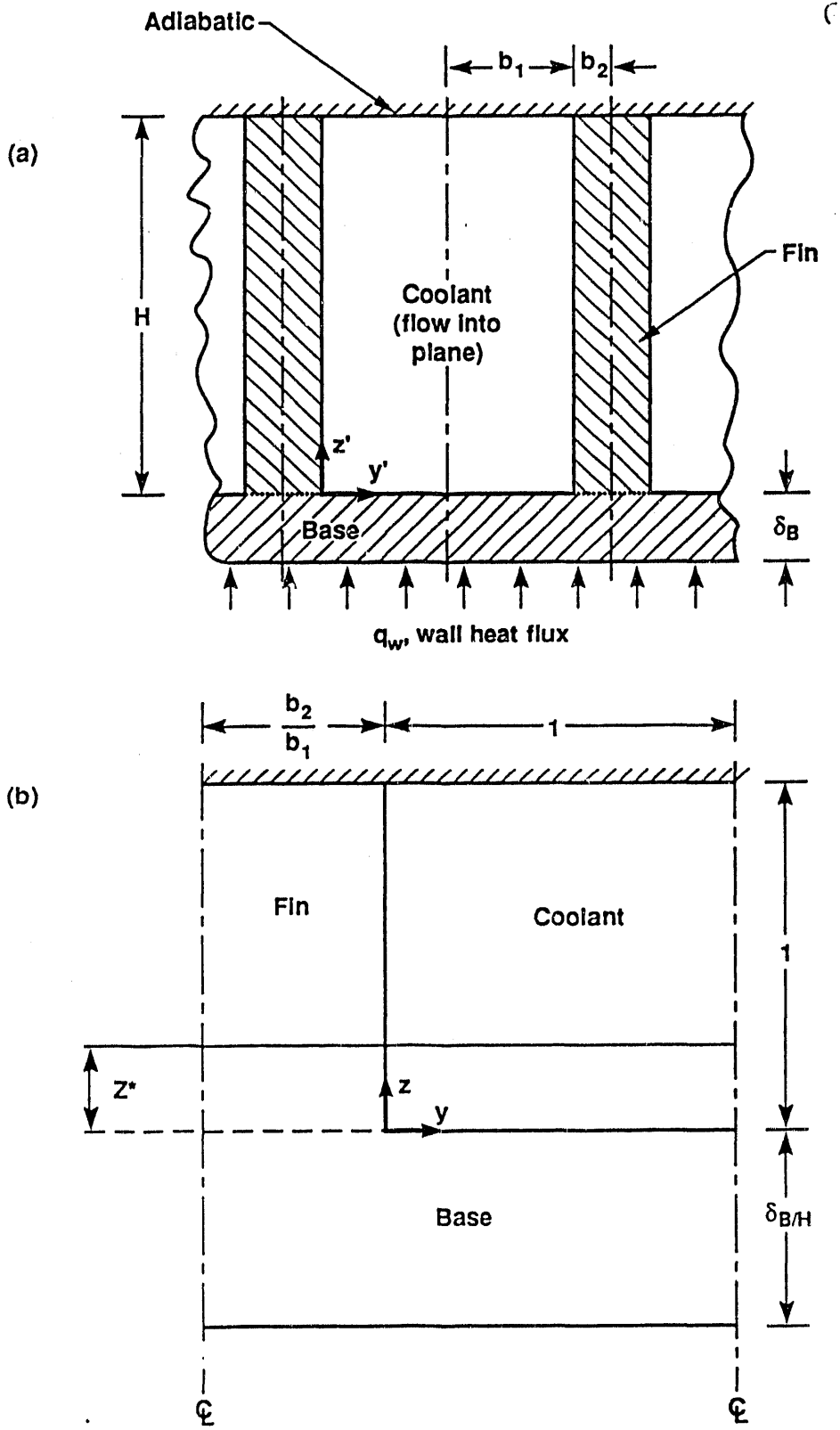
(a)
Adiabatic
b_1
b_2
H
Coolant
(flow into
plane)
Fin
z'
y'
Base
δ_B
q_w, wall heat flux
(b)
$\frac{b_2}{b_1}$
1
Fin
Coolant
1
Z*
z
y
Base
$\delta_{B/H}$
℄
℄

Fig 2

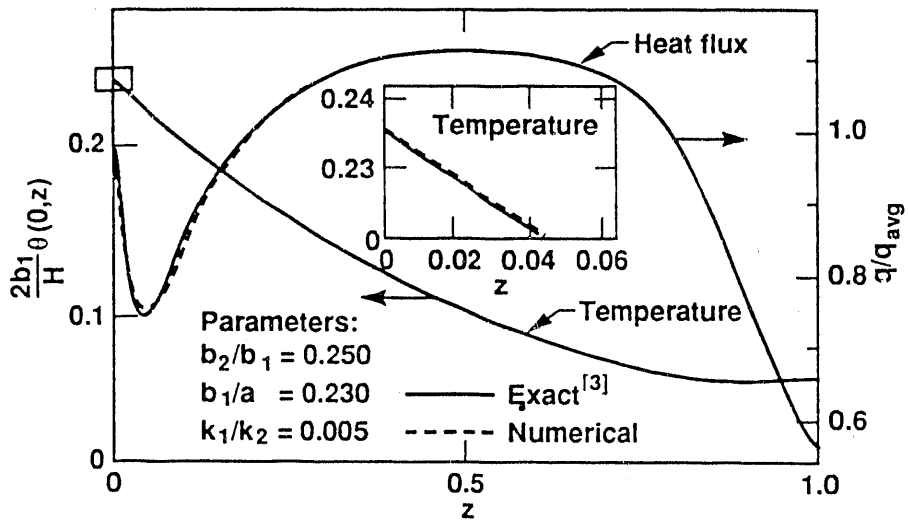
Heat flux
Temperature
Temperature
0.24
0.23
0
0 0.02 0.04 0.06
z
0.2
0.1
0
$\frac{2b_1}{H}\theta(0,z)$
1.0
0.8
0.6
q/q_{avg}
Parameters:
$b_2/b_1 = 0.250$
$b_1/a = 0.230$
$k_1/k_2 = 0.005$
Exact[3]
Numerical
0
0.5
1.0
z

Fig 3

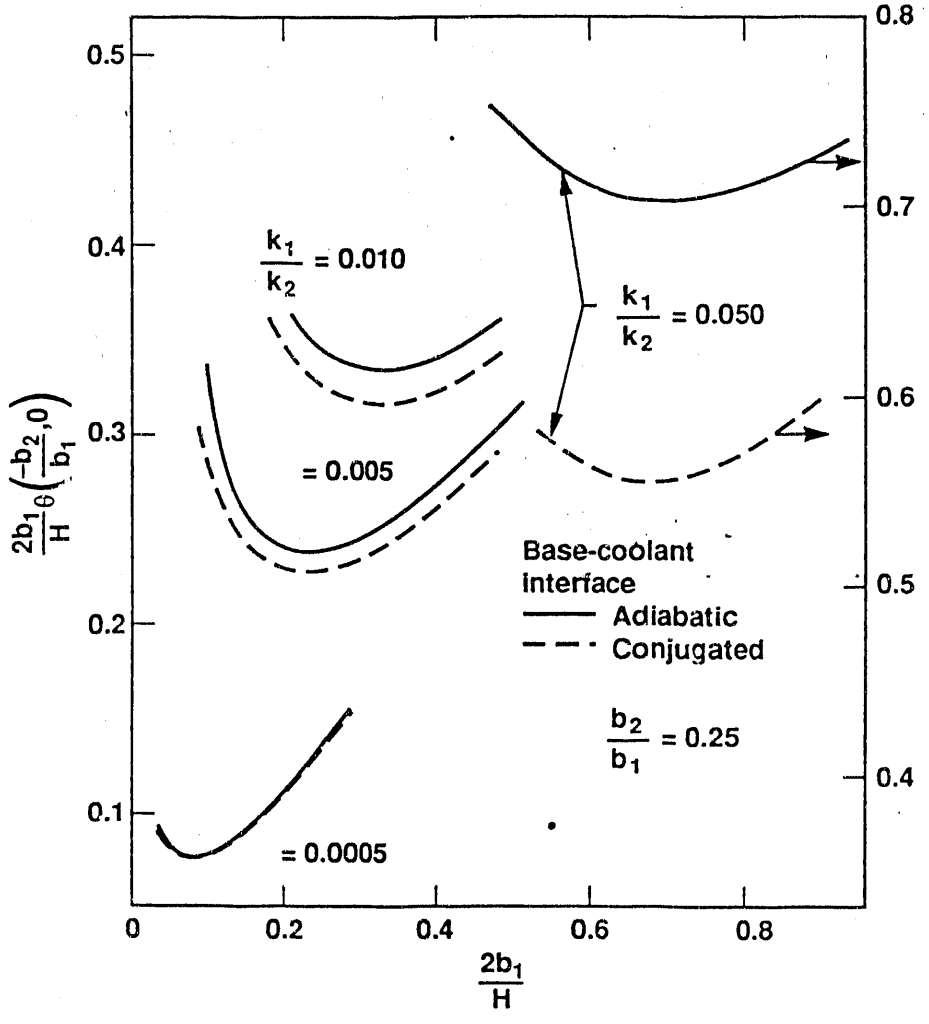
0.8
0.5
0.7
0.4
$\frac{k_1}{k_2}$ = 0.010
$\frac{k_1}{k_2}$ = 0.050
0.6
0.3
= 0.005
$\frac{2b_1}{H}\theta\left(\frac{-b_2}{b_1},0\right)$
Base-coolant
interface
Adiabatic
Conjugated
0.5
0.2
$\frac{b_2}{b_1}$ = 0.25
0.4
0.1
= 0.0005
0
0.2
0.4
0.6
0.8
$\frac{2b_1}{H}$

Fig 4

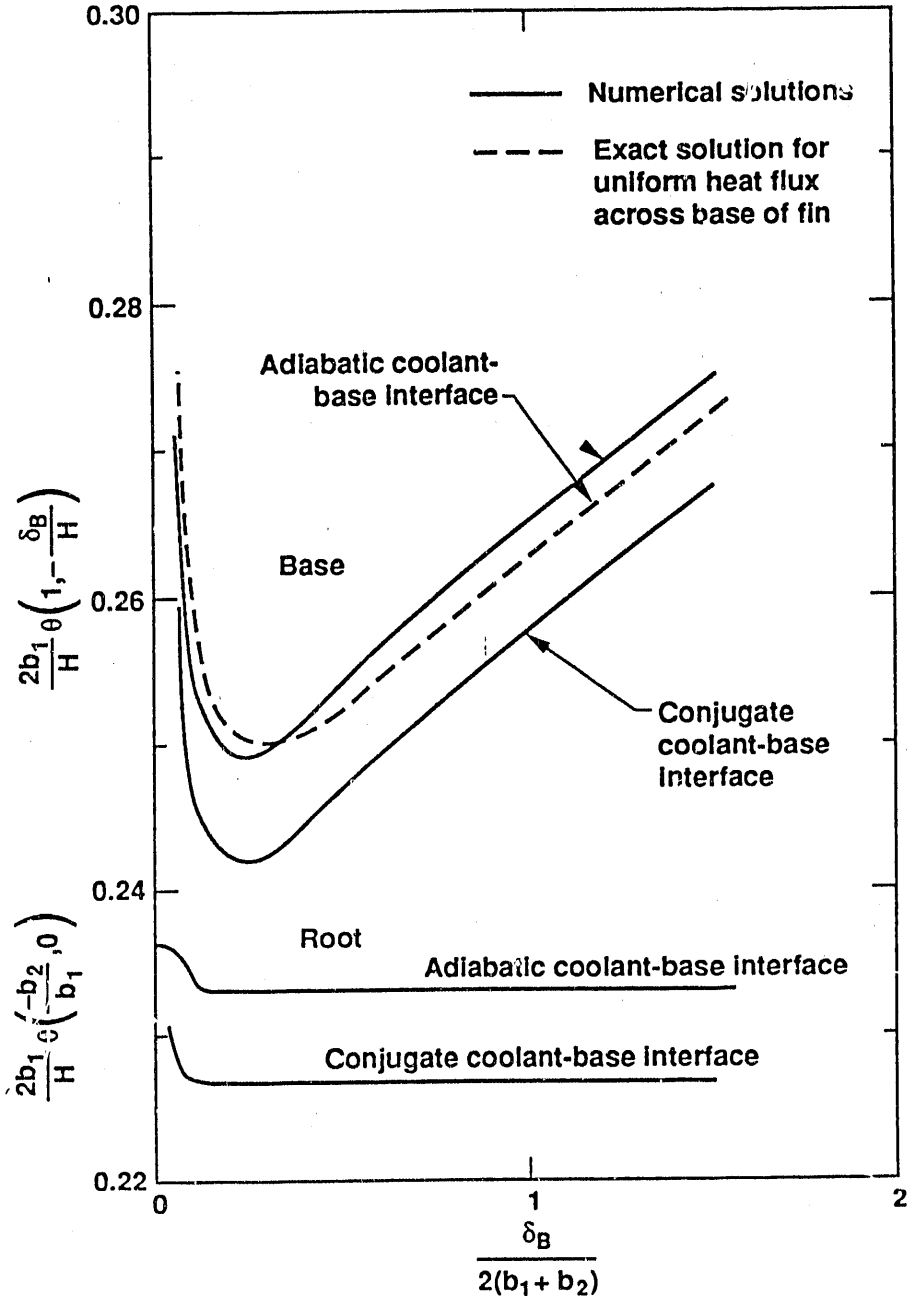
0.30
0.28
0.26
0.24
0.22
0
1
2
Numerical solutions
Exact solution for uniform heat flux across base of fin
Adiabatic coolant-base interface
Base
Conjugate coolant-base interface
Root
Adiabatic coolant-base interface
Conjugate coolant-base interface
$\frac{2b_1}{H}\theta\left(1,-\frac{\delta_B}{H}\right)$
$\frac{2b_1}{H}\theta\left(\frac{-b_2}{b_1},0\right)$
$\frac{\delta_B}{2(b_1+b_2)}$

fig 5

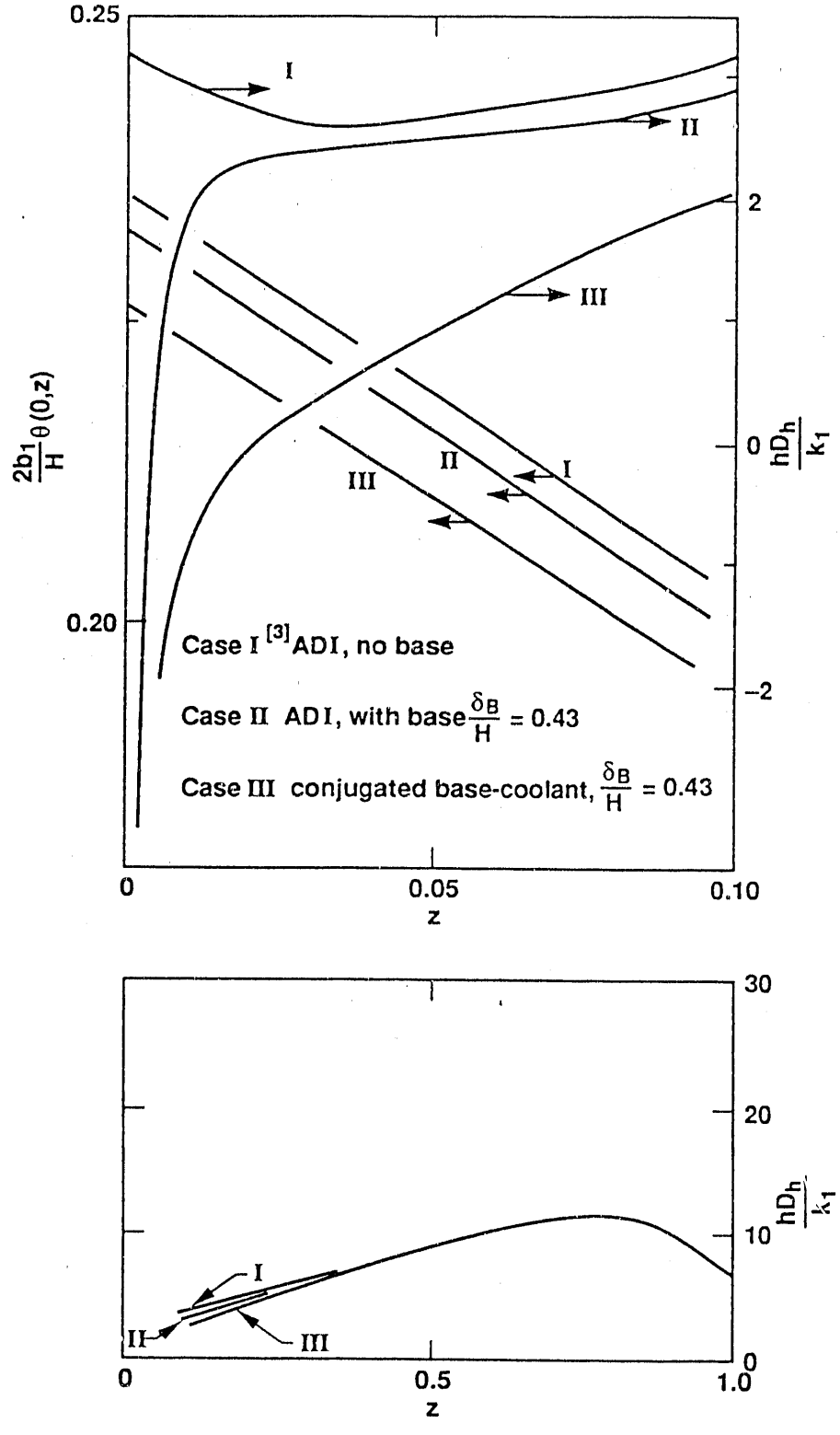
0.25
0.20
I
II
III
2
0
−2
$\frac{2b_1}{H}\theta(0,z)$
$\frac{hD_h}{k_1}$
Case I [3] ADI, no base
Case II ADI, with base $\frac{\delta_B}{H} = 0.43$
Case III conjugated base-coolant, $\frac{\delta_B}{H} = 0.43$
0
0.05
0.10
z
30
20
10
0
0.5
1.0

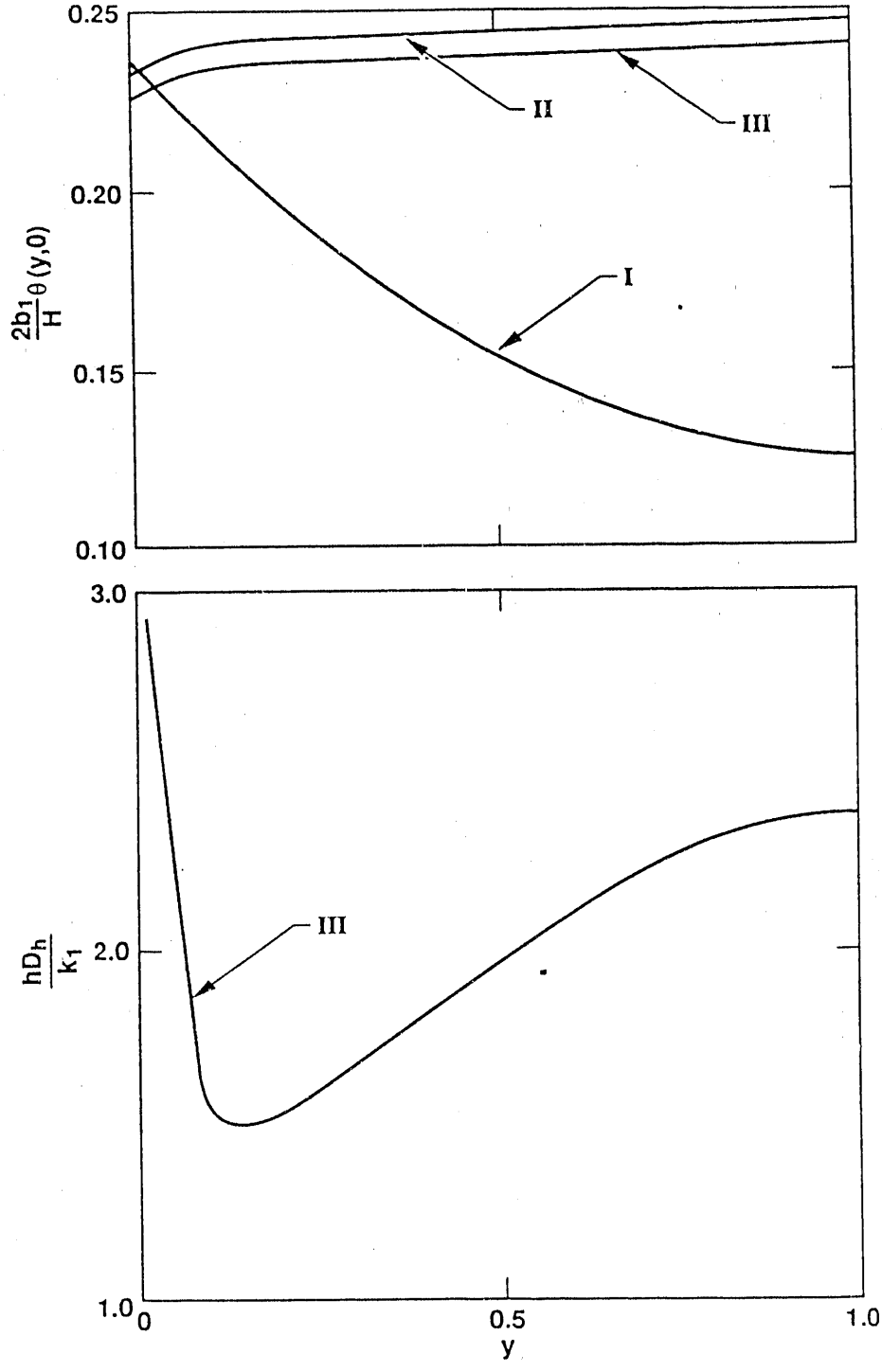
0.25
0.20
0.15
0.10
$\frac{2b_1}{H}\theta(y,0)$
II
III
I
3.0
2.0
1.0
$\frac{hD_h}{k_1}$
III
0
0.5
1.0
y

Fig 7

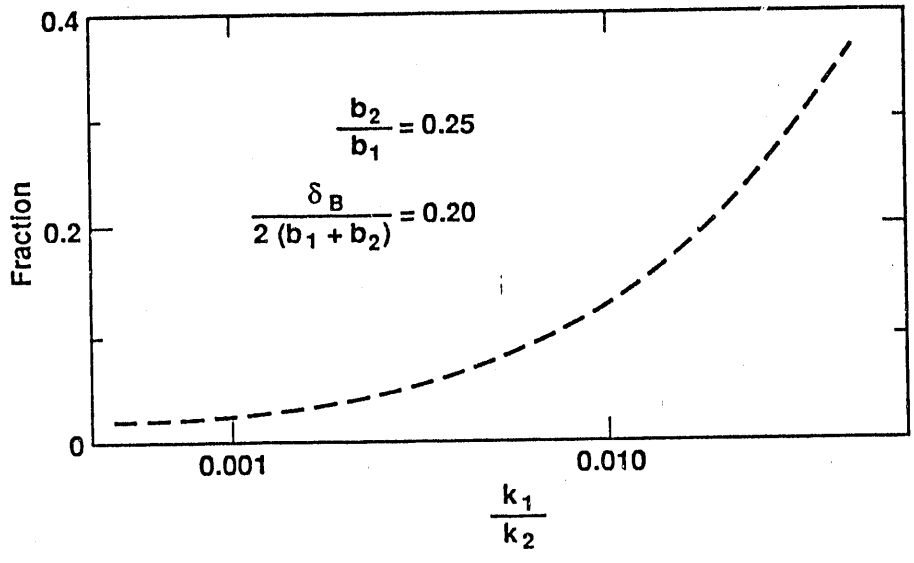
0.4
0.2
0
Fraction
$\frac{b_2}{b_1} = 0.25$
$\frac{\delta_B}{2(b_1 + b_2)} = 0.20$
0.001
0.010
$\frac{k_1}{k_2}$

Fig 8

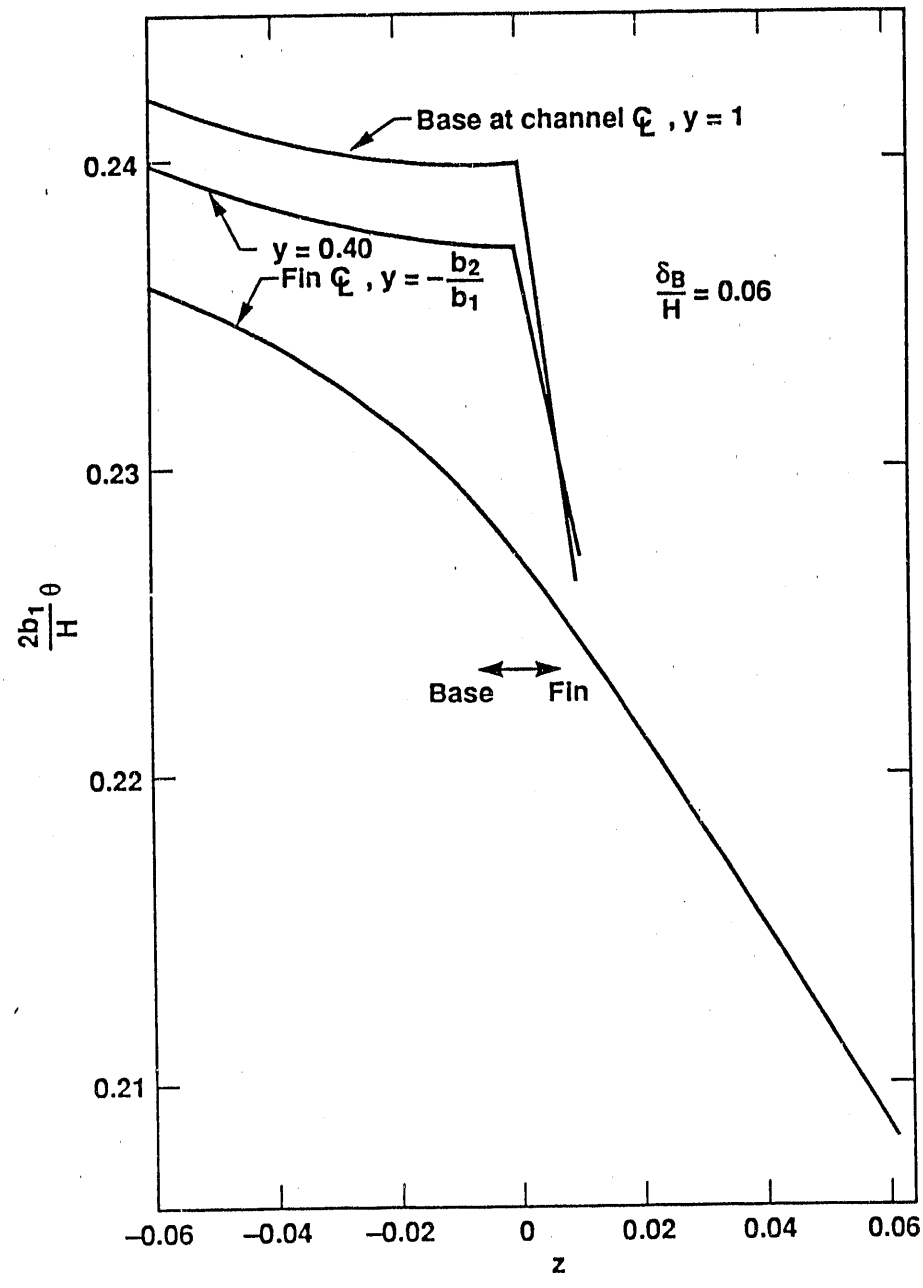
Base at channel ℄ , y = 1
y = 0.40
Fin ℄ , y = −b2/b1
δB/H = 0.06
Base
Fin
0.24
0.23
0.22
0.21
2b1/H θ
−0.06
−0.04
−0.02
0
0.02
0.04
0.06
z

Fig 9

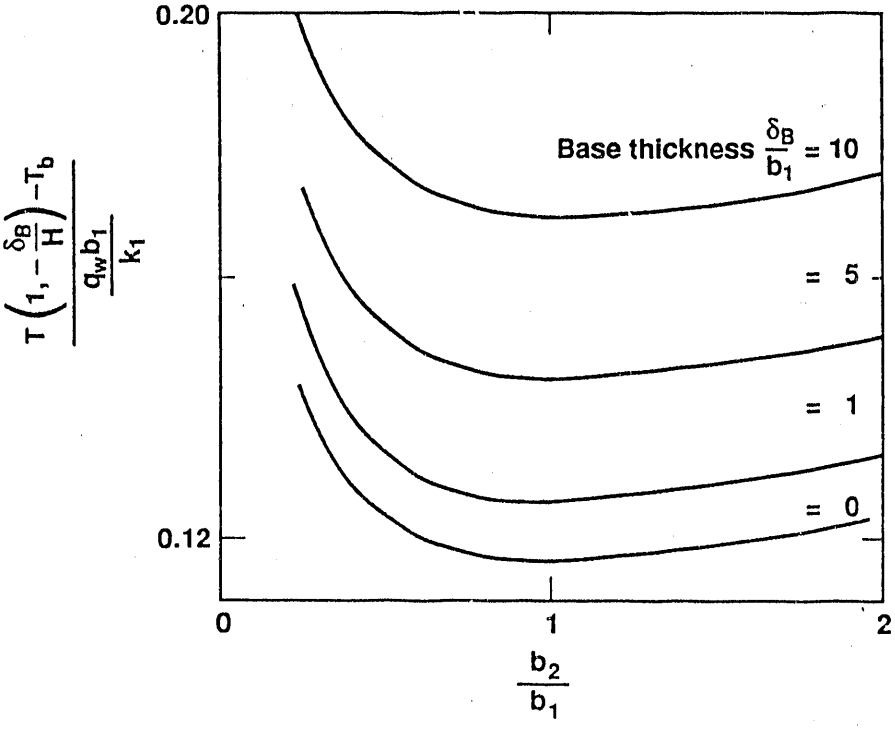
0.20
0.12
Base thickness $\frac{\delta_B}{b_1}$ = 10
= 5
= 1
= 0
0
1
2
$\frac{b_2}{b_1}$
$\frac{T\left(1,-\frac{\delta_B}{H}\right)-T_b}{\frac{q_w b_1}{k_1}}$

END

DATE FILMED

06 / 07 / 91